Int J Adv Manuf Technol (2015) 80:1077–1085
DOI 10.1007/s00170-015-7103-5

ORIGINAL ARTICLE

Strain path dependence of the FLC_0 formability parameter in an interstitial free steel

Marcos Domingos Xavier[1,2] · Nelson Batista de Lima[3] · Ronald Lesley Plaut[4] · Cláudio Geraldo Schön[4]

Received: 8 December 2014 / Accepted: 30 March 2015 / Published online: 14 April 2015
© Springer-Verlag London 2015

Abstract This work aims at studying the influence of the strain path upon the FLC_0 formability parameter, the root of the forming limit curves (FLC). The investigation was conducted in an interstitial free (IF) quality steel. The FLC_0 parameter was evaluated in an intrinsic tensile test in near plane strain (NPS) condition, but following two strain paths. The first one being a uniaxial (proportional) path up to initial necking. The second (non-proportional) path corresponded to applying 15 % nominal plastic strain in one direction (near plane strain) followed by a second deformation applied in the orthogonal direction up to the rupture of the samples. A reduction in the limit strains corresponding to FLC_0 in the non-proportional test has been observed. The forming limit stress curves (FLSC) and the critical values $FLSD_0$ are also related to these trajectories. A simulation using finite element method (FEM) has been applied to analyze the evolution of stress and strain during the two paths, and the results have been found consistent for both proportional and non-proportional paths. Texture and surface roughness evolution of the sheet were also measured and related to the applied strain paths.

Keywords Materials processing · Plane strain · Strain path · Strain FLC · Non-proportional loading · Texture

1 Introduction

Forming limit curves (FLCs), or, alternatively, forming limit diagrams (FLDs), have been introduced by Keeler and Backofen [1] and Goodwin [2] in the 1960s, as an empirical tool for evaluation of sheet metal formability in stamping processes. This tool, combined with the, so called, "circle grid analysis", would provide an efficient way of stamping failure-free parts and to project the corresponding dies [3, 4]. Soon, however, it was realized that the FLC is not a material property, rather it depends on many extrinsic factors; among them, the strain path through which deformation is produced [5]. In spite of being naturally connected with stamping, FLCs may be successfully applied to other processes which use sheet metal as raw material, like hydroforming [6] and hot forming [7].

In addition to that, it must be recognized that the most critical deformation condition in sheet metal forming is the plane strain state, which corresponds to a minimum in all FLCs. This leads to the concept of the FLC_0 parameter,

✉ Cláudio Geraldo Schön
schoen@usp.br

Marcos Domingos Xavier
mdxavier@fatecsp.br

Nelson Batista de Lima
nblima@ipen.br

[1] Nadir Dias de Figueiredo, Escola SENAI, Rua Ari Barroso, 305 – CEP 06216 - 901 Osasco, SP, Brazil

[2] Faculdade de Tecnologia de São Paulo, Centro Estadual de Educação Tecnológica Paula Souza, Av. Tiradentes, 615 – CEP 01124 - 060 São Paulo, SP, Brazil

[3] Department of Materials Characterization, Instituto de Pesquisas Energéticas e Nucleares, Comissão Nacional de Energia Nuclear, Travessa R, 400 – CEP 05508-900 São Paulo, SP, Brazil

[4] Department of Metallurgical and Materials Engineering, Escola Politécnica da Universidade de São Paulo, Av. Prof. Mello Moraes, 2463 – CEP 05508-030 São Paulo, SP, Brazil

which corresponds to this minimum deformation [1]. Literature surveys in forming automotive parts show that about 80 % of the failures occur close to the plane strain condition [8, 9].

The determination of FLC_0, based on forming limit curves, relies on the use of standard tests like Marciniak's or Nakazima's, in which a punch is pressed against the sheet, deforming it [3, 4]. In this kind of test, based on a large number of tested samples, the sheet does not remain flat, but it is progressively curved as the test progresses (i.e., it is deformed out-of-plane). In addition, there is contact and sliding between the punch and the sample's surface, resulting in friction. Both factors result in overestimating the necking strains, and, hence, the FLC. As Abed-Meraim et al. [10] point out, this leads to a lack of reproducibility in the experimental determination of the FLCs. Two approaches may be devised to solve this lack of reproducibility, one is to rely on modeling and prediction of FLCs [10], the second is to develop new tests, which would be less affected by these extrinsic factors.

Alternative tests have been, therefore, developed which focus on the direct determination of FLC_0 using fewer flat samples in tensile loading, in which deformation is always kept in-plane and friction does not play a significant role [11–13]. In a recent work, Xavier et al. [14] compared the standard FLC obtained using Nakazima's test and a special tensile sample which induced fracture in near plane strain conditions, using two different steels, an interstitial free (IF) quality steel and AISI 1050 sheets. The results show that the in-plane test led to significant reduced fracture strains compared with the standard FLC and that the difference is more severe in the case of the IF steel, which is characterized by higher formability.

Another approach to overcome the strain path dependence of the FLCs is based on the (empirical) observation that this dependence vanishes when the true principal stresses in the sheet plane are plotted instead of the principal strains, leading to the concept of the forming limit stress diagrams (FLSDs) [5, 15–22]. Arrieux [15] showed that the FLSDs are intrinsic properties of the sheet metal and furnished a recipe on how to calculate the limit strains for complex strain paths out of these diagrams. Stoughton and Zhu [23] showed that the path independence of the FLSDs can be justified using theoretical models for necking. These authors attribute the strain-path dependence of the FLCs to "...the path dependent relationship between the stress and strain tensors as defined by the constitutive law" [23].

More sophisticated crystal plasticity models incorporate the influence of crystallographic texture in the sheet formability. Charca-Ramos et al. [24, 25], for example, developed a polycrystal plasticity model capable of predicting the evolution of Lankford coefficient and the forming limit curve based on a standard tensile test and on an initial orientation distribution function (ODF) measured for the steel sheet. The same research group reported results in simulations using this model and concluded that crystallographic texture play an important role in defining the limit strains close to the equibiaxial stretching [26].

The obtained FLC or FLSDs may be combined with simulations using finite element method (FEM) to model the actual drawing processes. This requires three basic material inputs [27]:

a. an yield criterion (e.g., Hill's 1948 criterion, as usual for steel sheets),
b. a constitutive relation (e.g., Hollomon's or Swifft's, as usual for steel sheets) and
c. the experimental FLC.

In order to avoid the limitations of FLCs, as mentioned above, the last input could be substituted by the FLSDs, an option which is available in modern FEM software. Several authors have used FEM simulation to validate different aspects of the FLC and FLSDs [13, 15, 28].

The aim of the present work is to test the strain path dependence of the nearplane strain test introduced by Xavier et al. [14] and to confirm that the corresponding limit stresses are indeed, strain path independent, comparing the results with FEM simulations of the deformed samples. This test is conducted in a IF class steel, a material which is primarily processed by sheet metal forming. In addition, the texture and surface roughness evolution in the sheets submitted to both strain paths are measured and discussed.

2 Material and methods

2.1 Material

The present investigation was conducted on a 0.75-mm-thick IF quality steel sheet supplied by BRASMETAL WAELHOLZ SA (São Paulo-SP, Brazil). Analyzed composition (furnished by the supplier) is given in Table 1.

The base mechanical properties of the sheet were also characterized by the supplier, both for the tensile properties (according to standard ABNT NBR 16284) and anisotropy ratios (according to standard ASTM E517). The results are reproduced in Table 2. In this table, r_{0°, r_{45°, and r_{90° represent the Lankford coefficients along, respectively, 0°, 45°,

Table 1 Analyzed composition (in weight %) of the IF steel

Fe	%C	%Mn	%Si	%P	%Al	%Ti
bal.	0.0015	0.117	0.0072	0.0100	0.0320	0.0530

Table 2 Summary of the mechanical properties of the investigated sheets, as received

Property	Value
Yield strength (σ_y)	178 MPa
Ultimate tensile strength (UTS)	336 MPa
Elongation (ε_f)	0.421
r_{0°	1.73
r_{90°	2.02
r_{45°	1.23
K	584 MPa
n	0.22

and 90° from the rolling direction (RD), and K and n refer to the parameters of Hollomon's equation:

$$\sigma = K\varepsilon^n \tag{1}$$

Using these data, the normal anisotropy ratio, $r_m = 1.552$, and the planar anisotropy ratio, $\Delta r = 0.323$, may be calculated [3, 4]. These values suggest good formability, but also imply in a large anisotropy.

2.2 Nearplane strain tests

The influence of the plastic strain path on points FLC_0 and $FLSD_0$ was investigated using a special tensile tests sample geometry which fractures close to a plane strain state. This geometry is based on a suggestion by Wagoner [12] and was employed in a previous work by the present authors [14]. Figure 1 shows the initial sample geometry used in all experiments.

The test procedure corresponds to:

1. Prerecording, via serigraphy, of a net of ∅ 2 mm circles in samples, dimensioned as indicated in Fig. 1.
2. Application of the strain paths.
    a. Path 1: performing plastic strains until rupture via uniaxial tensile loading in the large flat samples, along its length. These samples were prepared having their length set either parallel to the rolling direction (RD) of the sheet or transverse (TD) to this rolling direction, considering three replicas for each orientation.
    b. Path 2: in a first step a (near plane) engineering strain of ≈15 % either along RD (03 samples) or along TD (03 samples). The test is interrupted at this point and a smaller self-similar sample (dimensions scaled according to the 1:4 ratio) is machined with its length perpendicular to the direction of the initial prestrain, these smaller samples were then deformed until rupture. Figure 2 illustrates this procedure.

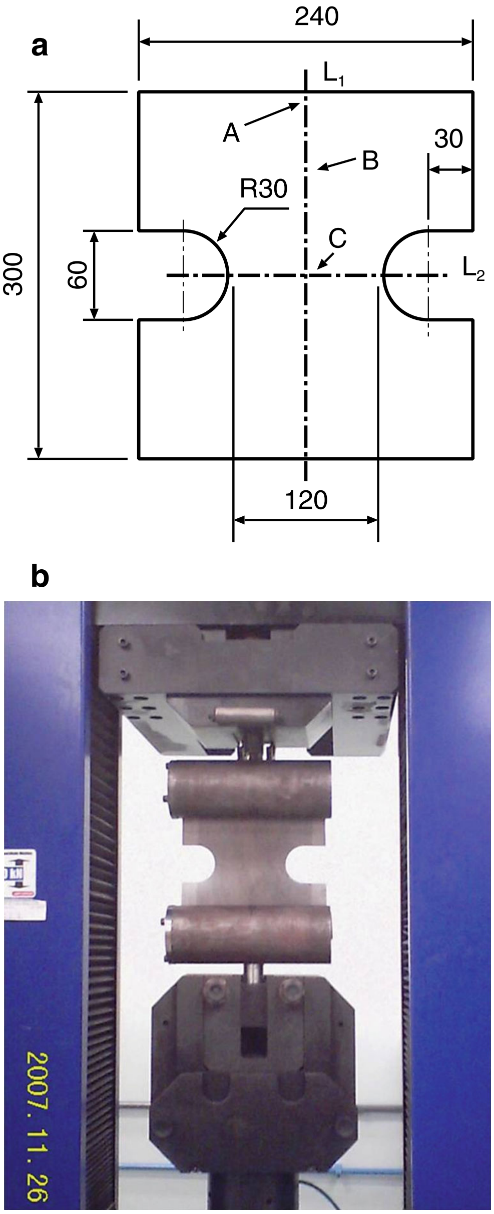

Fig. 1 Initial sample geometry employed in the tensile tests. **a** Dimensions: the two symmetry lines L_1 and L_2 which characterize the sample are defined, as well as the three regions (A, B, C) used for measurement of the surface roughness and **b** image of a sample attached to the testing machine

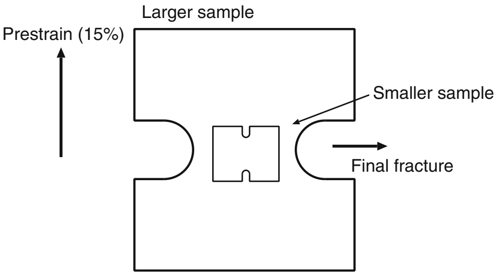

Fig. 2 Scheme for the extraction of the samples used for the second strain path

3. The ellipses generated by the plastic strains in both strain paths have been measured along the longitudinal axis of the samples for the determination of the major (d_1) and minor (d_2) axes. The corresponding true strains were calculated using:

$$\varepsilon_{1,2} = \ln \frac{d_{1,2}}{d_0} \tag{2}$$

The measurement of the circles adjacent to the necking region of the sample was made along longitudinal symmetry line L_1 (Fig. 1) averaging three parallel columns both to the left and to the right of such line (along symmetry line L_2 in the same Figure). The measurements associated with the three lateral columns on the left and on the right of the longitudinal line were made to increase the dimensional accuracy, eliminating discrepancies arising from possible sliding of the samples in the grips during the tensile tests.

In order to prevent damage in the sample's borders (increased roughness, presence of microcracks), all machining operations were performed using electrical discharge machining.

The principal stresses corresponding to the principal strains, measured in the necking region, were calculated using the procedure described by Stoughton [17], using Hill's 1948 yield criterion and Hollomon's constitutive equation, with the parameters of Table 2.

2.3 Finite element simulations

FEM simulations of the samples (both the larger and the smaller ones) were performed using the program AutoForm v. 4.07. Simulations followed the same strain paths applied to the experimental samples. The AutoForm program is a dedicated FEM algorithm, which was specifically written to model stamping processes [29]. The code is highly appreciated both in the industry and in the academy. Examples of applications are found in refs. [30, 31].

2.4 Texture and surface roughness analysis

The measurement of the surface roughness was performed using a Mitutoyo SJ-301 (2D) rugosimeter. Measurements were performed in three regions of the deformed samples, close to the necking area (A), at 1/4 length (B) and close to the machine grips (C). Surface roughness will be characterized using the average roughness (Ra) only.

Texture was measured by X-ray diffraction in a Rigaku DMAX Rint 2000 goniometer, belonging to the Instituto de Pesquisas Enenrgéticas e Nucleares/ Comissão Nacional de Energia Nuclear (IPEN/CNEN-SP), operating with a Molybdenum tube (Mo $K\alpha$ radiation wavelength, $\lambda = 0.071073$ nm). Four pole figures corresponding to planes (110), (200), (211), and (310) were acquired in 1 × 10 mm samples taken from the central region of the specimens and converted into orientation distribution functions (ODFs) using the Texture Analysis Program (PAT), developed by Galego [32]. The original sheet rolling direction was always used as reference for pole figure measurement and ODFs determination independent of the tensile sample orientation.

3 Results

3.1 Sheet formability in the near plane strain state

Table 3 shows the values of the principal true strains measured in the sheets oriented parallel to RD and perpendicular to this direction. In this table, the values marked "Path 1" and Path 2" correspond to the FLC_0 values measured in the proportional and non-proportional strain paths. The seemingly large limit strain for the proportional paths is consistent with the measured limit strains obtained by Tigrinho et al. in near plane strain conditions in steel DP600, which shows larger carbon content ($w_C = 0.08$) and slightly worse baseline mechanical properties ($n = 0.19$) [33].

The results of Table 3 are plotted in Fig. 3. Here, we observe that FLC_0 values for both deformation paths are only slightly anisotropic, but when compared, result in quite different formabilities. This result is consistent with the observed reduction of the FLCs for non-proportional deformation paths, reported in the literature (e.g., in refs. [5, 17, 18, 21, 34]).

Initially, empirical investigations by Keeler and Brazier [35] resulted in a relationship between the FLC_0 and sheet thickness (t in mm) and the strain hardening exponent (n) (the latter concerning the Hollomon equation):

$$FLC_0 = (23.3 + 14.2t) \times \left(\frac{n}{0.21}\right) \tag{3}$$

which is applicable to low carbon steels. Application to the present case suggests the failure would happen at $\varepsilon_2 = 0.0$ and $\varepsilon_1 = 0.356$, which is in reasonable agreement with the present results for Path 1. Alternative empirical approaches have been recently suggested by Abspoel et al. [36], but this

Table 3 Principal true strains measured in the samples originally oriented parallel to RD and perpendicular to RD (parallel to TD)

Sample	Orientation	ε_2	ε_1
Path 1	RD	-0.011	+0.370
≈ 15 %	RD	-0.004	+0.087
Path 2	⊥RD	+0.052	+0.107
Path 1	TD	-0.026	+0.409
≈ 15 %	TD	-0.011	+0.107
Path 2	⊥TD	+0.084	+0.120

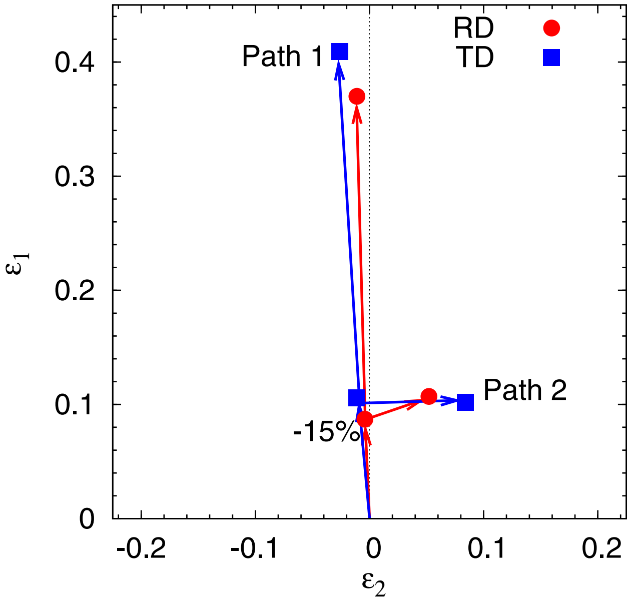

Fig. 3 Limit strains for the near plane strain tests in the investigated deformation paths as a function of sheet orientation

cannot be compared with the present case, since it is based on a material parameter which is not available for the here investigated steel. Naturally, the results for Path 2 cannot be compared with these empirical procedures, since they are designed for the FLC prediction, which is, by nature, limited to the case of a proportional strain path.

3.1.1 Forming limit stresses

The results obtained in the near plane strain tests may be converted into the corresponding forming limit stresses using the procedure suggested by Arrieux [15], which was later reviewed by Stoughton [17]. Table 4 presents the results of this procedure.

Table 5 shows the stresses (minor and major) obtained in the FEM simulations corresponding to Path 1 and Path 2. The values obtained for Path 1 are in agreement with the ones determined in the experiments (both in the RD and in the TD orientation). The resulting FEM stresses for Path 2, however, are clearly overestimated.

Table 4 Principal true stresses calculated for the samples originally oriented parallel to RD and perpendicular to RD (parallel to TD)

Sample	Orientation	σ_2 [MPa] (calc.)	σ_1 [MPa] (calc.)
Path 1	RD	384	624
≈ 15 %	RD	279	453
Path 2	⊥RD	318	517
Path 1	TD	391	636
≈ 15 %	TD	289	471
Path 2	⊥TD	338	550

Table 5 Limit stresses derived from the finite element simulations of deformation Paths 1 and 2, and calculated assuming the prediction of Keeler and Brazier [35] (KB)

Sample	σ_2 [MPa]	σ_1 [MPa]
Path 1	405	661
Path 2	360	684
KB	384	624

Figure 4 summarizes the results of FLSD_0 values in the near plane strain state, constructed based on the values obtained in the present work (both for the experimental results and for the FEM simulations) and the one calculate for Keeler and Brazier's prediction [35]. It is observed that there is agreement for the proportional deformation path (results from Path 1). However, in the case of the non-proportional path (Path 2), one observes that the calculated values are slightly lower than those observed in Path 1. This dependency does not need to be contradictory with the results reported by several authors (e. g., refs. [5, 15], which suggest a unique FLSD, which would be independent of the deformation path. A closer investigation of the present results suggest, indeed, that the points fall all (except for the FEM simulation of Path 2) onto a single curve (albeit the point corresponding to the plane strain condition is given by different coordinates in each case).

In the earliest experimental results [5, 15], the authors did not identify a single curve, but rather a narrow band of clustered curves, which could well be a consequence of the inevitable experimental and numerical errors associated with the critical stress evaluation, but could as well

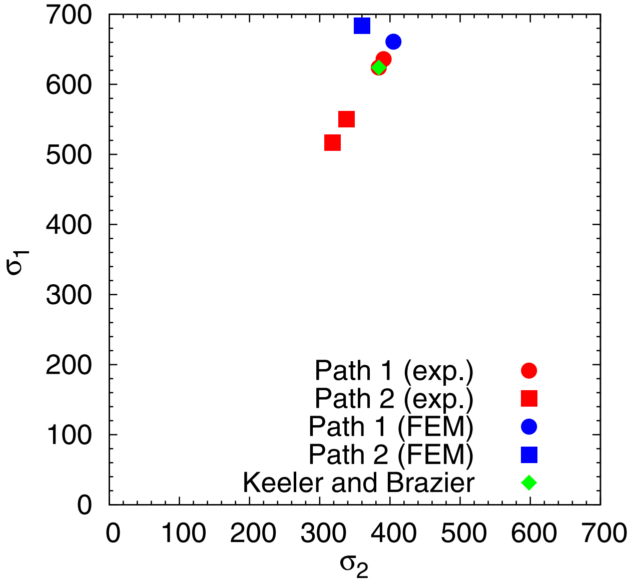

Fig. 4 Summary of the FLSD_0 values calculated base on the experimental (exp.), on the FEM simulations and derived from Keeler and Brazier [35] prediction

point out to a small but definite strain path dependency. These differences, if existing, could be associated with different microstructural aspects of the plastic deformation, such as occurrence of static recovery, variation in the crystallographic texture evolution, changes in surface roughness and some portion, due to the Bauschinger effect, linked to the development of deformation structure. Neither of these aspects are even considered in the present FLSD theory. Naturally, one cannot rule out the possibility that the calculation procedure is tainted by considering that the material is described by Hollomon's equation and that it yields according to Hill's criterion. Both hypotheses imply that the mechanical properties are not affected by plastic deformation, while it is well known that changes in n and r values are experimentally observed, depending on the strain level [37].

Kaluza et al. [38] experimentally determined FLSDs for several IF steels. Based on their compositions, we determine that the closest match the present steel is the one called "DC 06" in the original work. Comparing these results with the ones obtained in the present work, we observe that a good agreement is obtained (although based only on a very limited region of their full FLSD).

3.2 Surface roughness and texture

Table 6 shows the results of Ra measurements in the three regions of the larger specimen, as depicted in Fig. 1. As expected, average roughness increases with plastic deformation and is maximal in the necked region (region C in Fig. 1). The results are affected by sample orientation, with larger roughness in the case in which the sample is oriented along TD, suggesting that the initially isotropic surface pattern evolves in plastic deformation differently depending on the loading direction.

Table 7 shows the roughness evolution in region C (from Fig. 1) as a function of the deformation path. As expected, roughness increases, first from the initial value to the prestrain level ($\varepsilon = 0.15$) and then to necking according to the proportional strain path (Path 1) and the non-proportional strain path (Path 2). Interestingly, the increase in Path 2 is smoother compared with the increase in Path 1. This can be only a consequence of the larger deformation levels observed in Path 1, which imply larger dislocation activity. Comparing the sheets in RD and TD orientation, we see that anisotropy increases with deformation level and is maximal along Path 1.

Table 6 Surface roughness (in μm) in the larger samples, loaded until necking ensued (Path 1), in the three regions defined in Fig. 1

Orientation	Region A	Region B	Region C
RD	0.95 ± 0.02	1.02 ± 0.01	1.61 ± 0.02
TD	0.97 ± 0.03	1.27 ± 0.02	1.86 ± 0.01

Table 7 Roughness evolution (Ra in μm) in the necked region as a function of the strain path

Orientation	Original	Prestrain	Path 1	Path 2
RD	0.95 ± 0.01	1.21 ± 0.04	1.61 ± 0.02	1.30 ± 0.04
TD	0.97 ± 0.03	1.35 ± 0.09	1.86 ± 0.01	1.39 ± 0.06

Figure 5 shows the $\varphi_2 = 45°$ section of the orientation distribution function (ODF) of the samples characteristic from Path 1. As observed, the original sheet (Fig. 5a) is characterized by a well-developed γ fiber, probably to the finishing cold rolling passes performed by the supplier prior to delivery. Deformation along Path 1 in the RD orientation reinforces this fiber (Fig. 5b), this is expected since rolling is usually modeled as a plane strain process. A different result is obtained when the sheet is deformed along TD (Fig. 5c). In this case, the γ fiber disappears and is substituted by a discrete contributions around fiber $\{\bar{2}23\}$, but with smaller intensities (maximum 6.3 times random).

Analysis of the samples in deformation Path 2 (non-proportional) is shown in Fig. 6. The effect of the 15 % pre-strain is different whether deformation is applied along

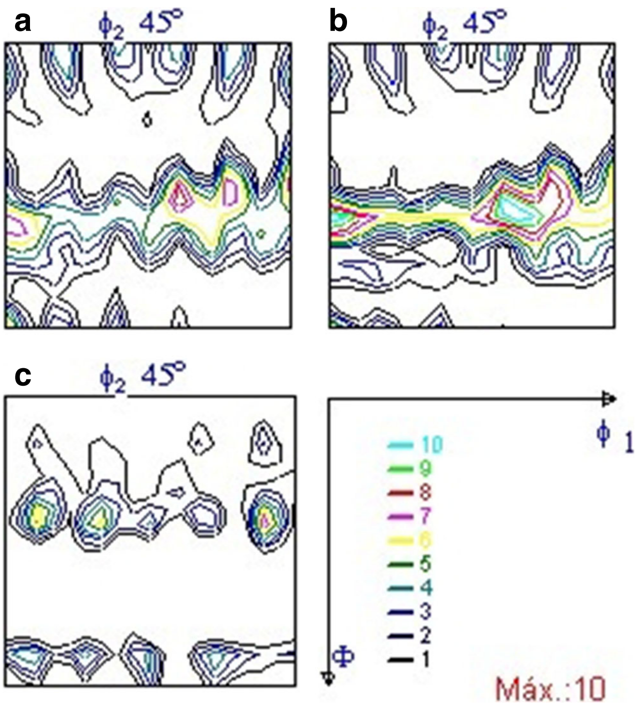

Fig. 5 Orientation distribution function ($\varphi_2 = 45°$ section) of the samples characteristic of Deformation Path 1 (proportional): **a** original sheet, **b** - necking region in a sample deformed along RD, **c** necking region in a sample deformed along TD

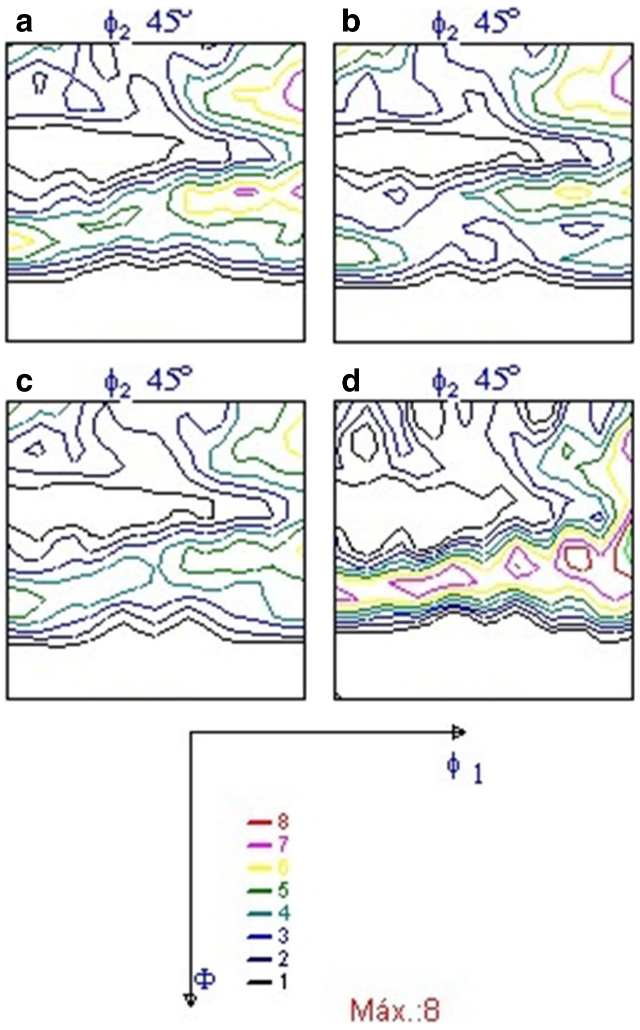

Fig. 6 Orientation distribution function ($\varphi_2 = 45°$ section) of the samples characteristic of deformation Path 2 (non-proportional): **a** after ≈15 % prestrain along RD, **b** after ≈15 % pre-strain along TD, **c** after ≈15 % prestrain along RD, followed by rupture along TD, and **d** after ≈15 % prestrain along TD, followed by rupture along RD

RD Fig. 6a or TD Fig. 6b. In both cases, however, the γ fiber is still recognized. Comparing with the original sample (Fig. 5a), we observe that the main features are preserved (e.g., the maximum intensity is observed around the same Euler angles in both Figures). In the case of deformation along TD, however, its maximum intensity decreased, while intensities close to the cube orientation increased. It appears that the 15 % prestrain along TD represents an intermediate step of the γ fiber dissolution observed in deformation Path 1 (Fig. 5c). The situation at rupture along Path 2 reinforces these differences. The sample which is initially prestrained along RD (and ruptured along TD) has a γ fiber which is further weakened and intensities close to the cube fiber increase (Fig. 6d)). In the sample which is initially prestrained along TD (and ruptures along RD), the γ fiber is further reinforced (Fig. 6d).

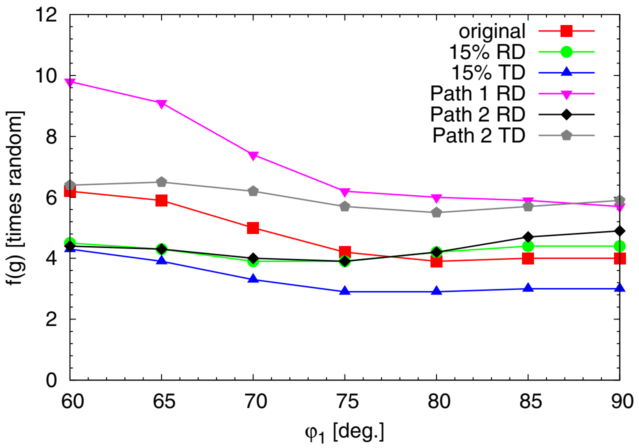

Fig. 7 Fiber plot for the γ fiber in selected samples, characteristic of the investigated strain paths

The results are summarized in Fig. 7, which presents the γ fiber plot of selected samples, characteristic of all strain paths investigated in the present work (expect for the case of Path 1 in the TD orientation, whose γ fiber has null intensity). The results show that whenever the sample is strained to fracture along RD (in Path 1 or in Path 2, for the sample which is initially prestrained along TD) the γ fiber is reinforced and a maximum intensity is observed at $\varphi_1 = 60°$ (orientation $[1\bar{1}0](111)$), the remaining sample present weaker, but more homogeneous γ fibers.

Comparing the texture results with the limit strains, shown in Fig. 3, we observe that the presence or absence of the γ fiber does not correlate with a better (or worse) formability. In fact, both in Path 1 (good formability) and Path 2 (limited formability), we have samples with strong and weak (or absent) γ fiber. A possible explanation for this result would be that the original blank already had a well-developed γ fiber. The prestrained samples, even in the cases where the sample is deformed along TD, show that this fiber is resistant to deformation. A strong γ fiber implies good formability, in the sense that it maximizes the presence of well-oriented slip systems across the blank thickness. The process of γ fiber dissolution occurs whenever the sample is deformed along TD, but its final disappearance would complete only in the late stages of deformation, when texture would no longer affect significantly the plastic deformation. This means that the good formability of the material, most probably, becomes compromised only at the late stages of deformation, where other effects rather than plasticity (like void growth and coalescence or strain localization) are dominant.

The results on sheet roughness also shows that its development correlates better with the extent of plastic deformation rather with texture evolution.

4 Conclusions

The use of the present sample geometry allows to conduct tensile test in near plane strain conditions, producing valid data for FLC_0 both in a proportional and in a non-proportional strain path for an IF steel. As already reported in standard FLC determinations, the FLC_0 values for the non-proportional strain path show significantly smaller limit strains compared with the proportional path. This means that a simplified test, not affected by extrinsic factors like friction between tool and sheet and out-of-plane deformation, which is considerably less time-consuming, is already able to reproduce the strain path dependence observed in a fully determined FLC.

The results of limit stresses, calculated based on the limit strains, are compatible with the concept of a unique forming limit stress diagram, which is independent of the strain path. The results, however, suggest that the locus of the plane strain fracture in these diagrams is dependent on the strain path. The utility of a FLSD for this kind of problem (locating the most critical limit deformations) becomes, therefore, weakened, since it is necessary to calculate how the principal stresses evolve in function of the deformation path. A FEM simulation based on the sample geometry and using the mechanical properties of the investigated steel corroborates the calculated stresses in the case of the proportional strain path only. Care should be taken in using this kind of simulation for non-proportional deformation paths.

The sample surface roughness of the samples was measured. Results show that surface roughness correlates with the deformation level only, both depending on position and on strain path. In particular sheet roughness appears to be insensitive to texture evolution, which is surprising. One possible explanation for this unexpected behavior would be that, as already discussed, texture evolves significantly only at the late stages of deformation, so these changes cannot affect significantly the surface roughness which is produced by a cumulative action of dislocations.

Texture, in most analyzed conditions, show a strong γ fiber, which is inherited from the original blank. Deformation along the rolling direction tends to strengthen this fiber, while deformation along the transverse direction has the opposite effect. The γ fiber weakening culminates in the case of the sample fractured in the proportional path along the transverse direction, in which the γ fiber is completely absent. Rolling deformation is essentially a plane strain deformation process, so, performing the plane strain tests along RD reinforces the basic phenomena which produce the γ fiber. Deformation along TD, however, finds a unfavorable microstructure, which evolves by redistributing the grain orientations in the sheet. These evolutions, however, do not correlate with the measured limit strains, which can be justified assuming these changes occur predominantly in the late stages of deformation, where they cannot affect the limit strains anymore.

Nomenclature

FLC	Forming limit curve
FLC_0	Root of the forming limit curve
FLD	Forming limit diagram
FLSD	Forming limit stress diagram
$FLSD_0$	Plane strain value of the FLSD
IF	Interstitial free (steel)
ODF	Orientation distribution function
UTS	Ultimate tensile strength
Δr	Planar anisotropy ratio
σ_y	Yield strength
$\varepsilon_{1,2}$	Major and minor strains
ε_f	Elongation
d_0	Original diameter of the circle grid
$d_{1,2}$	Major and minor axes of the deformed circles
K	Pre-factor of Hollomon's equation
$L_{1,2}$	Symmetry lines in the near plane strain sample
n	Strain hardening exponent
r_{α°	Lankford coefficient (oriented α° relative to RD
r_m	Normal anisotropy ratio
Ra	Average roughness
t	Sheet thickness

Acknowledgments The authors thank BRASMETAL WAELHOLZ S.A. (São Paulo, Brazil) for supporting the present work with raw material and chemical analysis. The assistance of Prof. José Roberto da Silva and Gilberto A. Varussa (Escola SENAI "Nadir Dias de Figueiredo", Osasco, Brazil) in different phases of the experiments is gratefully acknowledged. The authors are indebted to Profs. Enéias N. da Silva, Elias P. dos Santos and Guilherme de Moura (Escola SENAI "Theobaldo de Nigris", São Paulo, Brazil) for developing the serigraphic technique used in the present work. This work has been partially supported by the Brazilian National Research Council (CNPq, Brasília-DF, Brazil), process number 312424/2013-2.

References

1. Keeler SP (1994) J Mater Proc Tech 46:446
2. Goodwin G (1968) SAE Technical Papers (680093). doi:10.4721/680093
3. Meyers MA, Chawla KK (1999) Mechanical behavior of materials. Prentice Hall, Upper Saddle River-NJ
4. Schön CG (2013) Mecânica dos Materiais. Elsevier, Rio de Janeiro. (in Portuguese)
5. Zhao L, Soderby R, Sklad MP (1995) Int J Mech Sci 38(12):1307
6. Hashemi R, Faraji G, Abrinia K, Disaji AF (2010) Int J Adv Manuf Tech 46:551
7. Li F, Fu MW, Lin JP, Wang XN (2014) Int J Adv Manuf Tech 71:297

8. Drewes EJ, Floßdorf FJ, Freier K (1995) Stahl & Eisen 115(4):85
9. Hosford WF, Duncan JL (1999) JOM 51(11):39
10. Abed-Meraim F, Balan T, Altmeyer G (2014) Int J Adv Manuf Tech 71:1247
11. Ghosh AK, Hecker SS (1974) Metall Trans 5(10):2161
12. Wagoner RH (1980) Metall Trans A 11(1):165
13. Holmberg S, Enquist B, Thilderkvist P (2004) J Mater Proc Tech 145:72
14. Xavier MD, Plaut RL, Schön CG (2014) Mater Res 17(4):982
15. Arrieux R (1995) J Mater Proc Tech 53:47
16. Sing WM, Rao KP (1997) J Mater Proc Tech 67:201
17. Stoughton TB (2000) Int J Mech Sci 42:1
18. Chow CL, Yang XJ (2003) J Mater Proc Tech 133:304
19. Hari Manoj Simha C, Grantab R, Worswick MJ (2007) Int J Solids Struct 44:8663
20. Alsos HS, Hopperstad OS, Törnqvist R, Amdahl J (2008) Int J Solids Struct 45:2042
21. Stoughton TB, Yoon JW (2012) Int J Solids Struct 49:3616
22. Abushawashi Y, Xiao X, Astakhov V (2013) Int J Mech Sci 74:133
23. Stoughton TB, Zhu X (2004) Int J Plasticity 20:1463
24. Charca Ramos G, Stout M, Bolmaro RE, Signorelli JW, Turner P (2010) Int J Solids Struct 47:2285
25. Charca Ramos G, Stout M, Bolmaro RE, Signorelli JW, Bertinetti MA, Turner P (2010) Int J Solids Struct 47:2294
26. Serenelli MJ, Bertinetti MA, Signorelli JW (2011) Int J Solids Struct 48:1109
27. Ma B, Tieu AK, Lu C, Jiang Z (2002) J Mater Proc Tech 130-131:450
28. Nakamachi E, Xie CL, Harimoto M (2001) Int J Mech Sci 43:631
29. Kubli W, Reissner J (1995) J Mater Proc Tech 50:292
30. de Souza T, Rolfe BF (2010) Int J Mech Sci 52:1756
31. Bressan JD, Cieto JD, Vieira FH, Bastos LSB, Muñoz Rojas PA (2010) Int J Mater Form 3 Suppl 1:231
32. Galego E (2004) Desenvolvimento de programa computacional para tratamento de dados de textura pela técnica de difração de raios-X. Master's thesis, Instituto de Pesquisas Energticas e Nucleares. IPEN/CNEN-SP, São Paulo
33. Tigrinho LMV, Chemin Filho RA, Marcondes PVP (2013) Int J Adv Manuf Tech 69:1017
34. Uppaluri R, Reddy NV, Dixit PM (2011) Int J Mech Sci 53:365
35. Keeler SP, Brazier WG (1977) In: Kochysnky M (ed). Union Carbide Co., New York, pp 571–530
36. Abspoel M, Scholting ME, Droog JMM (2013) J Mater Proc Tech 213:759
37. Liewald M, Held C, Schleich R (2009) Steel Res 80(4):275
38. Kaluza W, Kim I, Bleck W (2002) Adv Eng Mater 4(4):191